ADVANCED ENGINEERING MATERIALS
www.aem-journal.com

Wet Chemical Treatment and Mg Doping of p-InP Surfaces for Ohmic Low-Resistive Metal Contacts

Masoud Ebrahimzadeh, Sari Granroth, Sami Vuori, Marko Punkkinen, Mikko Miettinen, Risto Punkkinen, Mikhail Kuzmin, Pekka Laukkanen,* Mika Lastusaari, and Kalevi Kokko*

Manufacturing a low-resistive Ohmic metal contact on p-type InP crystals for various applications is a challenge because of the Fermi-level pinning via surface defects and the diffusion of p-type doping atoms in InP. Development of wet-chemistry treatments and nanoscale control of p-doping for InP surfaces is crucial for decreasing the device resistivity losses and durability problems. Herein, a proper combination of HCl-based solution immersion, which directly provides an unusual wet chemical-induced InP(100)c(2 × 2) atomic structure, and low-temperature Mg-surface doping of the cleaned InP before Ni-film deposition is demonstrated to decrease the contact resistivity of Ni/p-InP by the factor of 10 approximately as compared to the lowest reference value without Mg. Deposition of the Mg intermediate layer on p-InP and postheating of Mg/p-InP at 350 °C, both performed in ultrahigh-vacuum (UHV) chamber, lead to intermixing of Mg and InP elements according to X-ray photoelectron spectroscopy. Introducing a small oxygen gas background ($O_2 \approx 10^{-6}$ mbar) in UHV chamber during the postheating of Mg/p-InP enhances the indium outdiffusion and provides the lowest contact resistivity. Quantum mechanical simulations indicate that the presence of InP native oxide or/and metal indium alloy at the interface increases In diffusion.

1. Introduction

Nowadays InP crystals are used in the industry in infrared detectors and laser diodes for example. InP crystals are also potential materials for high-speed radio-frequency transistor circuits, solar cells, quantum dot displays, field emission, and photodetection.[1–12] The common building block of most semiconductor devices is a metal–semiconductor junction which is used to transmit the electric current into a semiconductor crystal(s) like the p–n junction. Nanoscale control of the p-type and n-type doping of semiconductor crystals as well as the preparation of low-resistive Ohmic contact interfaces becomes more crucial for decreasing the resistive energy consumption and malfunctions in the devices.[13–20]

Fabrication of the ohmic contact for p-InP has been more difficult than for n-InP.[21–28] One established reason for the p-InP contact challenges is a relatively strong diffusion of p-type doping atoms (i.e., group-II elements) in InP at the growth and/or postheating temperatures. That leads to a variation in the doping concentration, which can for example cause a hole concentration decrease at p-InP surfaces and thus an increase in the contact resistance. Second, a semiconductor surface affects also the doping efficiency, changing the acceptor- or donor-level position in the bandgap.[29,30] Furthermore, the Schottky contact rather than the Ohmic junction is readily formed at metal/p-InP interfaces due to p-InP surface defects which cause the Fermi-level pinning, irrespective of the metal element.

Cleaning and passivation of III–V surfaces, which together form the first step in the contact fabrication to remove surface oxides and keep the surface clean, have been a significant challenge for decades for various III–V device interfaces (e.g., refs. [31–33]). Furthermore, meaning of this first step can be expected to increase when the size of used III–V crystals decreases.[5,7,18,19,34,35] A wet chemistry treatment of III–V crystals is undoubtedly the most used method for cleaning and passivation because it is simple and scalable. It is worth noting that surfaces of InP crystals are an interesting exception among III–V compounds because the native oxides of InP cause less optical and electrical degradation.[36,37]

M. Ebrahimzadeh, S. Granroth, M. Punkkinen, M. Miettinen, R. Punkkinen, M. Kuzmin, P. Laukkanen, K. Kokko
Department of Physics and Astronomy
University of Turku
FI-20014 Turku, Finland
E-mail: masoud.m.ebrahimzadeh@utu.fi; pekka.laukkanen@utu.fi

S. Vuori, M. Lastusaari
Department of Chemistry
University of Turku
Turku FI-20014, Finland

R. Punkkinen
Department of Computing
University of Turku
Turku FI-20014, Finland

The ORCID identification number(s) for the author(s) of this article can be found under https://doi.org/10.1002/adem.202300762.

DOI: 10.1002/adem.202300762

Several metals or metal alloys have been investigated for the Ohmic p-InP contact. For example, Au, Ni, Pt, Pd, and AuZn and AuBe alloys provided a decrease in the contact resistivity.[38–48] Among these, Pt and Ni have been widely used in the Si technology as well. Furthermore, using a Sb interlayer[48] before a metal film has led to the formation of InSb, which has a much smaller bandgap than InP, making the preparation of Ohmic contact easier. After metal film deposition, metal/InP junctions have been typically postheated around 400 °C, which might cause a problem because InP surfaces are relatively reactive and thermally unstable among III–V surfaces.

Because the Schottky-type band bending is common at a metal/semiconductor interface due to a high density of interface defects, increasing the doping concentration at the semiconductor surface is used to decrease the width of a possible depletion region (**Figure 1**) and make the carrier tunneling process probable.[13,40,44,49] One way to increase the doping level at semiconductor surfaces before the metal film growth is to deposit an intermediate layer of the metal, which can act as a p-type (or n-type) element, between the semiconductor and the main metal. During the postheating step(s), the metal/semiconductor elements can diffuse over the interface providing an interface structure where the doping metal atoms replace the host semiconductor element in proper manner, increasing finally the effective doping density. This strategy has been recently used successfully for p-type GaN which has also suffered from the high contact resistivity.[49] Magnesium (Mg) has been the traditional p-type doping element for the nitride semiconductors, while Zn and Be are often incorporated into other p-III–V's to replace the III lattice sites. The high postheating temperature around 800 °C, at which InP degrades strongly, was needed for Mg/p-GaN.[49]

In this work, we demonstrate that an effective Mg surface doping of InP can be done at 350 °C or lower when a proper hydrochloric acid (HCl)-based solution treatment is combined by engineering the Mg-covered InP surface in ultrahigh-vacuum (UHV) conditions. First, a proper HCl + isopropanol (IPA) immersion is shown to cause an unusual InP(100) surface reconstruction without any postheating or treatment in UHV. This surface was used as the template for depositing 1–5 nm-thick Mg film. Postheating a Mg/InP stack in a UHV chamber at 350 °C causes the diffusion of P and In toward the surface according to X-Ray photoelectron spectroscopy (XPS). Our quantum mechanical simulations clarify the factors behind the diffusion. Contact resistivity measurements of Ni/p-InP show that an optimized Mg surface doping decreases the resistivity to 1/10 of that for the reference sample without Mg.

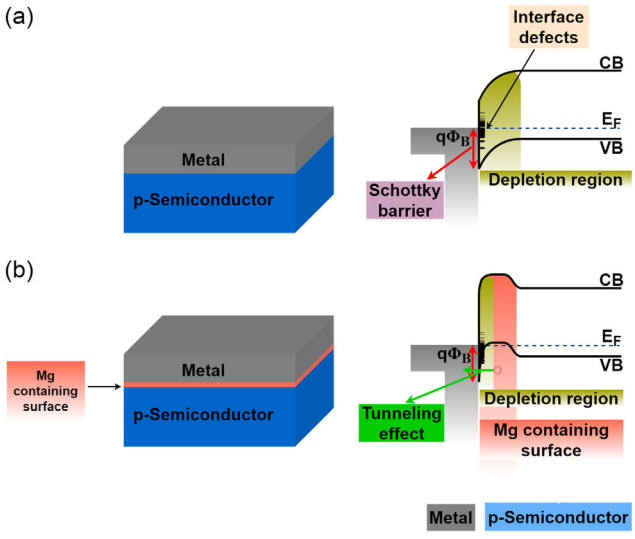

Figure 1. Schematic representation of the p-type surface-doping influence on the band diagram of the Schottky type metal and p-type semiconductor contact a) without and b) with Mg surface doping.

2. Results and Discussion

2.1. Effects of Wet Chemical Treatment of InP(100)

It is known that proper wet chemical treatment of a III–V surface removes most surface oxides (e.g., refs. [31,32]). When a wet chemically treated IIIV surface is quickly transferred into UHV environment, the surface shows diffraction intensity maxima in low-energy electron diffraction (LEED) or reflection high-energy electron diffraction (RHEED) characterization. Such a diffraction pattern is so-called (1 × 1), which arises from elastic electrons diffracted back from the bulk crystal planes below the topmost surface layer that still remains disordered or amorphous.[33] A fingerprint for crystallization of the topmost surface is a surface reconstruction, which varies among different III–V surfaces. The reconstruction means that the surface lattice changes as compared to the bulk-plane lattice, which can be readily observed in LEED or RHEED, because extra diffraction intensity spots appear. Usually, a (1 × 1) bulk plane structure is not energetically stable at the clean surfaces of semiconductor crystals, and the total energy of a crystal decreases via the surface reconstruction. However, the conditions in a wet chemical treatment do not typically enable a semiconductor surface to gain the minimum energy-reconstructed structure.

Furthermore, it is not straightforward to prepare and maintain a crystalline semiconductor surface because an amount of impurities such as oxygen and carbon increases at the surface with the time even in UHV environment. One common procedure to prepare a crystalline surface reconstruction is the heating of a III–V semiconductor surface, from which most oxides and impurities have been removed beforehand, in UHV conditions around 250–550 °C. The clean and crystalline surface of InP(100) shows the (2 × 4) reconstruction that consists of the dimer rows. Thermal stability of InP surfaces is relatively low among different III–V surfaces because P atoms start to evaporate from the surface in UHV above 400 °C, causing a visibly gray surface with metallic indium clusters.

Therefore, the result (**Figure 2**a) that a wet chemically treated p-InP(100) surface directly has a c(2 × 2) reconstruction without any postheating or treatment is very surprising. For an optimized treatment, p-InP crystal was immersed in 1 M (or 3%) HCl solution diluted with IPA for 5 min followed by 1 min immersion in pure IPA. According to our knowledge, there is no previous report on the formation of a wet chemically induced

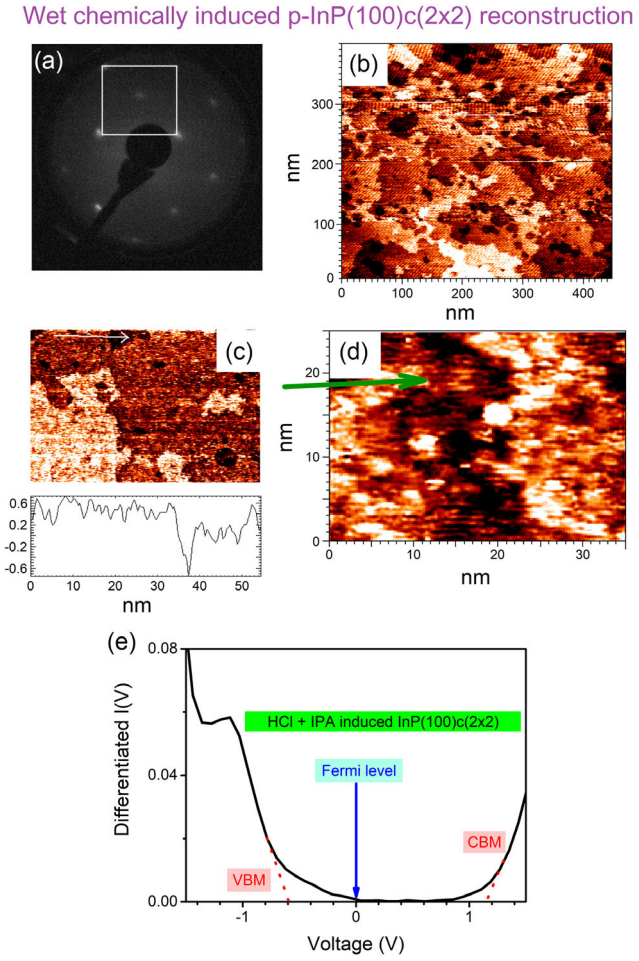

Figure 2. Wet chemistry-induced p-InP(100)c(2 × 2) reconstruction characterized just after the chemical treatment in UHV chamber without any postheating or treatment. a) LEED pattern represents the reciprocal lattice of c(2 × 2); white square marks the bulk-plane (1 × 1) unit cell, and the white dot in the middle of the square is a fingerprint of c(2 × 2). b) Large-scale STM image shows the formation of smooth 2D terraces. c) Contour line profile along the white arrow indicates that a height separation between lower and higher terraces is about 0.3 nm, which corresponds to a thickness of one InP layer. d) Zoomed STM image shows the presence of local horizontal lines, which can be linked to ×2 periodicity in real space. (e) Differentiated STS I(V) curve measured, which is proportional the electronic density of levels at the surface, showing that the surface is p-type.

long-range-ordered reconstruction on a III–V semiconductor without any extra treatment (e.g., postheating). The c(2 × 2) lattice is also unusual because the (2 × 4) reconstruction is the energetically favored structure at InP(100), but c(2 × 2) resembles the previously found hydrogen-induced InP(100)(2 × 1) surface.[50] Thus it is probable that the found c(2 × 2) reconstruction includes hydrogen as well. XPS results below indicate that the c(2 × 2) surface also contains more P than In. The presence of hydrogen is supported by the observation that the extra c(2 × 2) diffraction spots in LEED disappear, according to our observations, when the surface is bombarded by the LEED electrons for prolonged times.

Large-scale scanning-tunneling-microscopy (STM) images (Figure 2b,c) reveal that the p-InP(100)c(2 × 2) surface consists of smooth 2D terraces indicative of a crystalline topmost surface. A zoomed STM image in Figure 2d shows a local periodic structure of horizontal lines. It is possible that the STM tunneling current also breaks the reconstruction, as the LEED electron bombardment did. Scanning tunneling spectroscopy (STS) curve in Figure 2e indicates that no significant band bending downward occurs at p-InP(100)c(2 × 2) because the Fermi level lies in the bottom part of the bandgap.

Thus, the metal contacts prepared on the p-InP(100)c(2 × 2) starting surface provided a stringent reference sample for Mg surface doping tests presented below. It is worth noting that the above-described surface-science sample was transferred after the wet chemistry via air (in 10 min) to the UHV chamber, but it is expected that the hydrogen termination of p-InP(100)c(2 × 2) decreases the rate of oxygen-atom incorporation into InP. However, as presented below, this p-InP(100)c(2 × 2) sample transferred via air caused O 1s signal in XPS, indicating that it is very difficult to avoid oxygen incorporation into a semiconductor surface in practice even if a full oxide layer is not yet formed. Furthermore, according to our experiments, a HCl concentration of the etching solution affects the resulting surface structure because an increased HCl concentration from 1 to 3 M caused boat-like pits at the p-InP(100) surface (Figure S1, Supporting Information).

2.2. Effect of Mg Surface Doping on Ni/InP Resistivity

Figure 3 exemplifies the transfer length method (TLM) where Ohmic current–voltage lines are measured as a function of the metal pad distance. Then total resistance is plotted as a function of the distance (Figure 3c), and the y-axis intercept of a linear line gives a value of $2R_c$, where R_c is the contact resistance. The contact resistivity (ρ_c) is determined by the equation

$$\rho_c = R_c W L_T \tag{1}$$

where W is a width of the metal contacts and L_T is a characteristic contact length, which is determined by the x-axis intercept of the linear resistance–distance line. The x-axis intercept value is $-2L_T$.

Table 1 summarizes different samples and contact resistivities. All samples contained 100 nm Ni film of which contacts were patterned using lithography and excess metal was etched by 2 M HCl solution. All these "as-ready" contacts (Table 1) were measured first and then postheated for 60 min in UHV environment at 250 °C and remeasured. The surface treatment varied before the Ni film deposition (Table 1). The reference Sample A included the above-described p-InP(100)c(2 × 2) starting surface for Ni growth. The postheating of Ni/p-InP at 250 °C in UHV decreased the resistivity significantly, 27 times to $5.3 \times 10^{-5}\ \Omega\,cm^2$, which was the lowest value among different reference samples (Table S1, Supporting Information). Characteristic contact lengths and contact resistances of the samples are given in Table S2, Supporting Information.

Thickness of a Mg intermediate layer, deposited on the p-InP(100)c(2 × 2) surface, varied between 1 and 5 nm in our experiments. The postheating of Mg/p-InP at 350 °C for

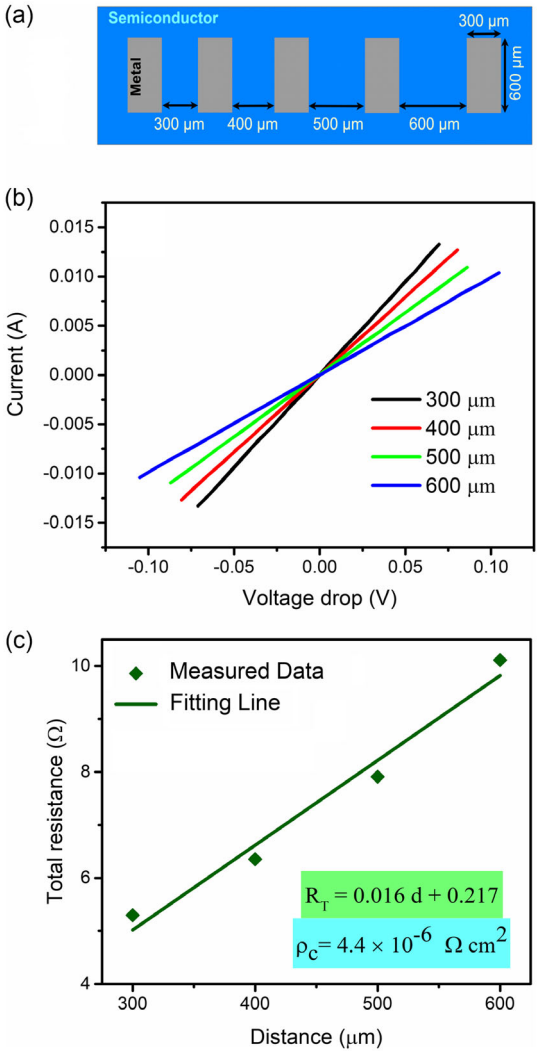

Figure 3. a) Top-view schematic representation of a TLM structure. b) Example of current as a function of voltage drop on the pad distance for Sample F (4 nm Mg + annealed with O_2 gas exposure). c) Resistance–distance dependence determined by TLM method.

60 min was performed in the same UHV multichamber instrument without air exposure. According to STS (Figure S2, Supporting Information), this Mg surface doping moves the Fermi level toward the valence band as expected if the p-type doping increases at the surface. Mg/p-InP samples were transferred via air (≈15 min) to a Ni growth instrument. Before the Ni deposition by sputtering, the Mg/p-InP samples were still etched in hydrofluoric acid (HF) solution (3 M or 5%) to remove an extra unreacted Mg from the surface (Figure S3, Supporting Information).[49]

Table 1 shows that incorporating 3 or 4 nm-thick Mg layer into the interface (Sample C or D, respectively) decreases the as-ready contact resistivity as compared to pure Ni/p-InP. However, the 250 °C postheating did not decrease the resistivity as much as it did for the reference Sample A. The resistivity after the post heating was higher for Sample C and lower for Sample D, as compared the reference Sample A.

When the postheating of Mg/p-InP was done in oxygen (O_2) background of 1×10^{-6} mbar controlled by a leak valve in the UHV chamber, the final resistivity decreased for Sample E (3 nm Mg) and F (4 nm Mg). The lowest resistivity value in these experiments was $4.4 \times 10^{-6}\ \Omega\,cm^2$ which was obtained using the 4-nm Mg intermediate layer and O_2 background during heating Mg/p-InP. This contact resistivity is among the lowest values reported in literature for p-InP, as listed in **Table 2.** One difference between this study and many previous ones is that we decreased the postheating temperature because InP crystals are known to be vulnerable to elevated temperatures, for example, causing doping atom and indium diffusion. Future studies can clarify if the presented approach decreases the contact resistivity for thin p-InP layers grown or implanted. In order to clarify the interfacial reactions that occur during post heating of Mg/InP and Ni/InP, and that can be linked to the contact resistivity changes, we have carried out XPS measurements and theoretical simulations.

2.3. X-Ray Photoelectron Spectroscopy of p-InP Interfaces

Figure 4a shows atomic concentrations derived from XPS spectra for Ni (4 nm)/p-InP sample as a function of sputtering time.

Table 1. Summary of different Ni/p-InP samples prepared in this work.

Sample	Chemical cleaning of p-InP	Mg deposition [nm]	Post heating of Mg/InP	HF (5%) dip time before Ni growth [s]	Ni film thickness [nm]	Etching solution	Contact resistivity [$\Omega\,cm^2$]	
							As-ready	Post heating in UHV [250 °C–60 min]
A	HCl (1 M or 3 %) for 5 min + IPA dip for 1 min + dried with N_2	–	–	–	100	HCl (2 M or 6 %)	1.4×10^{-3}	5.3×10^{-5}
B		1	350 °C - 60 min without O_2 ambient	5			3.5×10^{-3}	2.6×10^{-3}
C		3		10			1.2×10^{-4}	1.3×10^{-4}
D		4		10			4.3×10^{-5}	2.0×10^{-5}
E		3	350 °C - 60 min in O_2 ambient	10			1.5×10^{-4}	5.9×10^{-5}
F		4		10			2.9×10^{-5}	4.4×10^{-6}

Table 2. Comparison of p-InP contact studies found in literature. Heating time is given either in minutes or seconds.

Year	Temperature [°C]	Heating time [min]	Doping concentration [cm^{-3}]	Metal	Contact resistivity [$\Omega\ cm^2$]	References
1979	446	50	6×10^{17}	Au-Mg	1×10^{-4}	[64]
1980	420	10	$\leq 1 \times 10^{18}$	Au-Be	7.8×10^{-5}	[65]
1981	400	2	9×10^{17}	Au-Zn	1.1×10^{-4}	[22]
1982	425	30	1.3×10^{18}	Au-Be	2×10^{-4}	[66]
1988	410	90 s	10^{18}	Au-TiW-Au-Zn	3.7×10^{-5}	[67]
1991	440	20 s	5×10^{18}	AuZn	7×10^{-6}	[68]
1991	440	20 s	5×10^{18}	Au-AuZn	1.4×10^{-5}	[68]
1991	430	20 s	5×10^{18}	Au-Ni-AuZn	2.7×10^{-5}	[68]
1991	420–425	30–75 s	2×10^{18}	Au-Pd-Zn-Pd	7×10^{-5}	[39]
1996	500	1	2×10^{18}	Zn-Pd	4×10^{-5}	[40]
1996	500	1	2×10^{18}	Pd(Zn)-Ge	4×10^{-5}	[69]
1997	500	1	2×10^{18}	Pd-Sb-Zn-Pd	2×10^{-6}	[70]
1999	300	3	$1–4 \times 10^{18}$	Ni-Zn-Ni	7×10^{-5}	[38]
2000	375–400	2	2×10^{18}	Sb-Zn-Pd	7×10^{-5}	[41]
2002	375	2	$4–5 \times 10^{18}$	Pd-Zn-Pd	3×10^{-4}	[71]
2002	375–400	2	$4–5 \times 10^{18}$	Sb-Zn-Pd	7×10^{-5}	[71]
2005	400	4	$\approx 10^{18}$	Au-Pt-Zn-Pd	7×10^{-6}	[72]
2006	450	3	high 10^{18}	Au-Zn-AuZn	2.8×10^{-6}	[73]
2021	380	1	2×10^{18}	Au-Pt-Ni	2.64×10^{-6}	[74]
2023	250	60	$\approx 10^{18}$	Ni-Mg	4.4×10^{-6}	Current work

Figure S4, Supporting Information, presents the corresponding Ni 2p, O 1s, In 3d, and P 2p spectra. The sputtering removed the material from the top of Ni but did not remove the Ni film completely. Before XPS, the Ni (4 nm)/p-InP sample was postheated at 250 °C in UHV for 60 min. The topmost Ni surface was oxidized in air during the sample transfer before UHV heating. The concentration of outdiffused indium at the topmost oxidized Ni surface is about three times higher than the amount of outdiffused P (Figure 4a). Higher diffusion (or accumulation) of In toward the Ni surface has been found also previously.[51] The topmost surface of Ni/p-InP includes both the oxidized In and P atoms in addition to NiO_x (Figure S4, Supporting Information). However, when the oxidized Ni part is removed, the In concentration decreases. Simultaneously, the P signal becomes larger than the In signal, but this does not necessarily mean that the amount of P is higher than the In amount inside of the Ni film. In other words, the In 3d and P 2p electrons have different surface sensitivities (i.e., mean free paths), causing changes in the intensity contribution from the InP side below the Ni film, which has not been taken into account here in the determination of atomic concentrations. Obviously, alloying of Ni and InP occurs already at 250 °C, which can be associated with the heating-induced decrease in resistivity (Table 1). This is discussed more.

The concentration profiles of outdiffused In and P (Figure 4b) are rather different for Mg(4 nm)/p-InP sample, which was post heated in situ after at 350 °C in O_2 background for 60 min in the UHV chamber. The formed MgO layer at the top is thicker than NiO_x. Furthermore, the amounts of outdiffused In and P are lower at Mg/p-InP compared to Ni/p-InP. A strong tendency toward the oxidation of Mg can be also seen in **Figure 5**, which shows that the O 1s intensity increases even during the postheating of Mg/p-InP in UHV without intentional O_2 background. Furthermore, the amounts of outdiffused In and P are rather equal at the top of Mg/p-InP according to Figure 4b.

Figure 5 shows changes in in situ XPS measurements of In $3d_{5/2}$, P 2p, and O 1s for Mg(4 nm)/p-InP after the postheating at 350 °C for 60 min in the UHV chamber. The two different environments: UHV and O_2 of 1×10^{-6} mbar were used during the post heating of Mg/p-InP. The Mg/p-InP samples were not exposed to air before 350 °C heating. It can be seen in Figure 5 that both In and P atoms diffuse rather equally toward the topmost surface because their intensities increase after the UHV heating, taking also into account that the starting InP(100) $c(2 \times 2)$ surface is P rich. In contrast, the O_2 background during the postheating increases relatively the In $3d_{5/2}$ intensity more than P 2p intensity. The results suggest that the presence of oxygen background or/and surface oxides decreases the P outdiffusion more than the indium outdiffusion. These results can be associated with the reduced resistivity due to the O_2 background (Table 1) because the outdiffused In atoms can provide the lattice sites for Mg doping atoms at the InP surface. To understand factors behind the observed diffusion, theoretical simulations have been performed.

Ab initio molecular dynamics (AIMD) simulations reveal surprisingly that the diffusivity of the P atoms is larger than that of the In atoms in the metallic Ni crystal. This is partly due to the fact that the P atoms occupy interstitial positions, whereas In

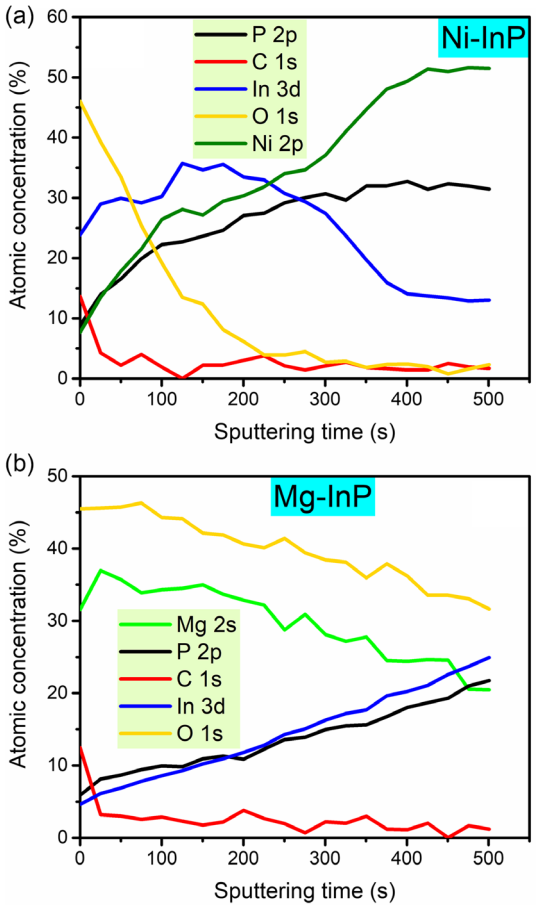

Figure 4. XPS depth profile measurements of atomic concentrations as a function of sputtering (etching) time for a) Ni(4 nm)/InP, which was transferred via air and postheated at 250 °C in UHV for 60 min and b) Mg(4 nm)/InP, which was post heated at 350 °C in UHV for 60 min with O_2 background. After sputtering, both samples still included a metal film.

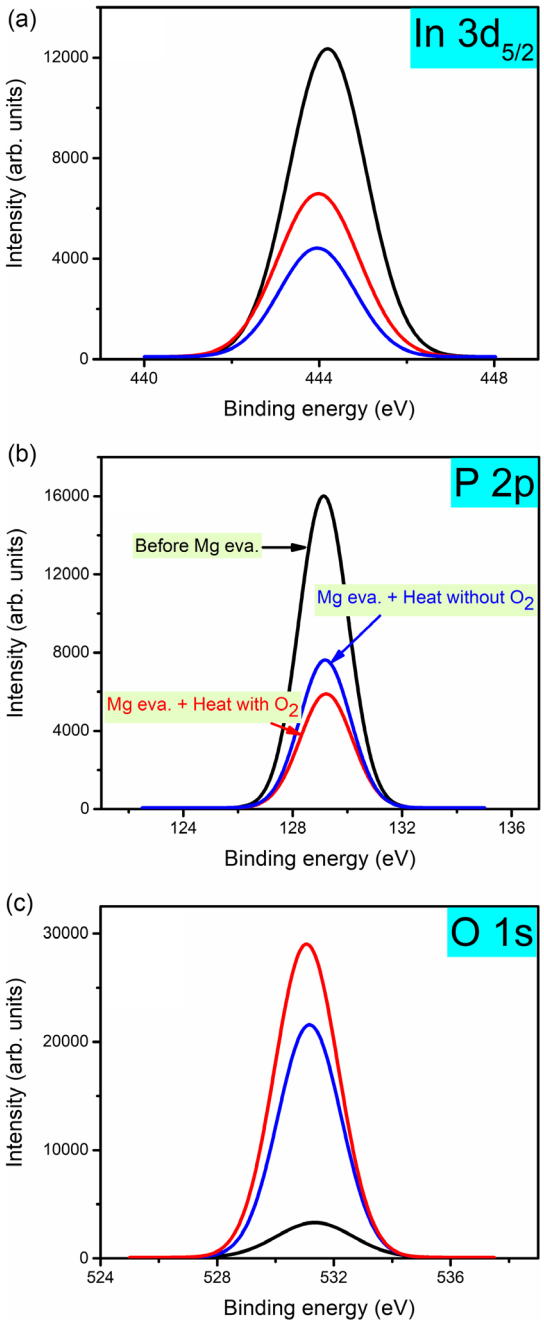

Figure 5. Effect of O_2 background during heating of Mg(4 nm)/p-InP at 350 °C for 60 min. a) In 3d with and without O_2 ambient. b) P 2p with and without O_2 ambient. c) O 1s with and without O_2 ambient.

occupies substitutional positions in Ni crystals. Therefore, the different diffusivities of In and P inside the Ni crystal are not the reason for the higher In concentration at the top of Ni/p-InP (Figure 4a), although a clear P amount has also diffused to the top of Ni/p-InP. However, the simulation result suggests that the interfacial mixing or alloying of elements starts with the diffusion of P toward Ni. The diffusivity of the P atoms is larger also in the metal oxides of NiO and MgO, in which In atoms occupy substitutional Ni and Mg lattice sites, whereas P atoms occupy substitutional O lattice sites. However, the diffusivities of the In and P atoms are more similar in pure Mg crystal, which is consistent with the concentration measurements in Figure 4b.

Furthermore, the self-diffusivity of the interstitial In atoms is larger than that of the interstitial P atoms in $InPO_4$, which is the thermodynamically most stable oxide of InP. This result is in agreement with the former experimental conclusions about indium diffusion.[52,53] It is worth noting the cleaned InP surface becomes partially oxidized during the sample transfer to the Ni growth instrument. The interstitial In atoms kick other In atoms to interstitial sites by substituting them in the $InPO_4$, as presented in **Figure 6**. This result suggests also that the diffusivity of indium increases with increasing In concentration in other mixed systems (e.g., In_xNi_y containing alloy), because heavy In atoms are able to kick other In atoms.

The XPS and theoretical results suggest that at the Ni/InP interface, the outdiffusions of P and In atoms proceed via the different interfacial phases: P atoms diffuse through pure Ni or/and NiO while the In outdiffusion increases with the

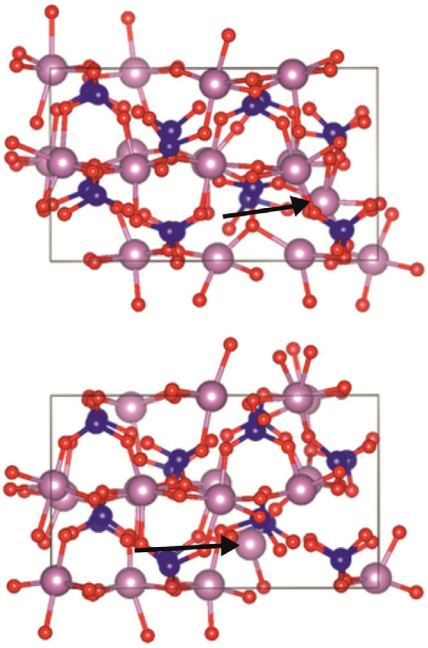

Figure 6. Atomic models of $InPO_4$ with interstitial In of which position is shown by black arrow. Violet, blue, and red spheres represent In, P, and O atoms, respectively.

formation of $InPO_4$ and In_xNi_y-containing interface phases. The interfacial reactions, which can initiate via P diffusion into Ni, are enhanced by postheating, after which more In than P has outdiffused (or accumulated) toward the Ni surface. Concomitantly, the postheating decreases significantly the contact resistivity of Ni/p-InP (Sample A in Table 1). This can be understood by the formation of indium vacancies in the InP side, which are expected to cause p-type electron levels in the gap near the valence band maximum.[54] In contrast, at Mg/p-InP, equal outdiffusion can be expected for In and P atoms if the metallic Mg layer at the interface is thick enough, while the MgO phase formation increases the P outdiffusion. The XPS concentration profiles in Figure 4 suggest that the elemental intermixing at Mg/p-InP is not as strong as at the Ni/p-InP interface (i.e., Mg/p-InP is less alloyed than Ni/p-InP). The presence of O_2 background gas in the postheating of Mg/p-InP can enhance the In outdiffusion, which is expected to provide more the free In lattice sites for Mg atoms, in consistency with the resistivity decrease for the Sample F in Table 1. Future studies are needed to clarify the effects of oxygen on the formation of p-InP contacts. Intuitively, the interfacial oxides can be expected to increase the contact resistance, but on the other hand, proper interfacial oxides have been found to decrease the contact resistance for example at p-GaN and 2D semiconductors.[17,55,56]

In addition to the contact resistivity, surface recombination of the electric carriers is a relevant property to describe performance of the metal/semiconductor contacts. In other words, lower surface recombination means a higher quality of the contact interface. Usually, it is difficult to decrease both the resistivity and surface recombination simultaneously at metal/semiconductor interfaces because the metal–semiconductor

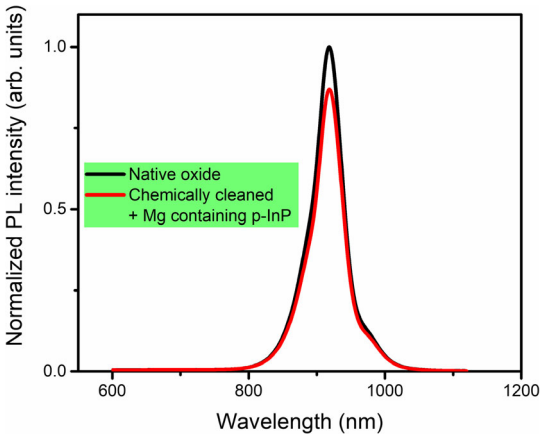

Figure 7. PL intensity comparison of p-InP with a native oxide surface and with Mg surface doping. The shoulder around 1000 nm is expected to arise from the transitions through acceptor levels in the bandgap.

alloying (e.g., elements diffusion in post heating) as well as a high doping atom concentration increases formation of defect-induced gap levels. For example, the P vacancies and both In and P antisites in InP can cause the deep gap levels.[54]

Therefore, we studied the photoluminescence (PL) intensity of p-InP to test whether the Mg surface doping described above increases the harmful surface recombination. The higher PL intensity means less surface recombination. The PL from native oxide-covered InP crystal has been used here as the reference because it provides surprisingly strong PL (i.e., high-quality reference intensity) as compared to many other III–V crystals with the native oxide.[36] The PL intensity comparison in **Figure 7** indicates that the Mg surface doping does not increase much the surface recombination. This Mg/p-InP sample was not etched in the HF solution after the UHV treatments to avoid any additional PL improvement due to possible hydrogen passivation.

3. Conclusion

We have demonstrated that the combination of wet chemistry and UHV-based surface doping of p-InP is a potential low-temperature method to decrease the contact resistivity in InP devices. Surprisingly the HCl-based wet chemical treatment produces directly a surface reconstruction on p-InP(100) without any post-treatment. The discovered p-InP(100)c(2 × 2) surface contains hydrogen termination, according to previous reports,[50] and provides a high-quality reference contact of Ni/p-InP for our study. This reference resistivity can be still decreased to 1/10 when at 4 nm-thick Mg intermediate layer and in situ UHV heating in oxygen background are used in the fabrication of Ni/p-InP contacts. The quantum mechanical calculations explain the XPS measurement of outdiffusion profiles for In and P atoms as follows. The presence of the interfacial $InPO_4$ and In_xNi_y-containing phases increases the In outdiffusion while the pure Ni, NiO, and MgO phases enhance the P outdiffusion.

4. Experimental Section

The experiments were conducted with 6×12 mm^2 pieces of Zn-doped InP(100) wafer with a dopant concentration of $\approx 10^{18}$ cm^{-3}. Chemical etching of the samples was performed with either HF- or HCl-based solution diluted with IPA. HCl-based cleaned samples were then soaked in IPA for 1 min and finally dried with N_2. Then they were loaded in the UHV system for different surface treatments and measurements. The UHV system consists of two chambers: preparation (with a base pressure of high 10^{-9} mbar) and analysis (with a base pressure of low 10^{-10} mbar). Deposition of Mg layers was conducted using a direct current-heated Ta envelope evaporator. To calibrate the deposition rate, Mg was deposited on the top of Si(100) pieces and attenuation of Si 2p XPS signal was measured. Then, Mg layer depositions were done on the wet chemically cleaned InP surfaces. Following that, the Mg/p-InP samples were heated in situ for 60 min in a UHV chamber with or without an O_2 gas background. The pressure during heating in O_2 background was 1×10^{-6} mbar. To remove any surface oxide or an unreacted part of Mg prior to Ni deposition, the Mg/InP samples were dipped into HF (3 M or 5%) for 10–15 s, which was expected to provide H termination layer also, just before Ni growth. All samples were transferred via air for the deposition of 100 nm nickel (Ni) using Bal-Tec MCS 020 sputter. The specific contact resistivity (ρ_C) was determined using the TLM method. TLM structures with various spacing pads were fabricated using photolithography and chemical etching. Finally, the Ni/InP contacts with and without Mg were post heated at 250 °C for 60 min in the UHV system.

To investigate chemical and physical properties of the surfaces, both in situ and ex situ techniques were used. In situ techniques included (Mg–Kα) nonmonochromatic XPS, LEED, and STM/STS, while ex situ XPS was done with monochromatized (Al–Kα) Thermo Scientific Nexsa. An argon ion beam with an energy of 300 eV was applied to the surface for removing part of Ni or Mg film. The area of this Ar sputtered surface was 0.5–0.7 mm^2 with an elliptical shape. The STM measurements were performed in constant-current mode using the Omicron Scala instrument. In STS, the current–voltage curves were measured in grid mode, which were then averaged over the selected regions and finally differentiated. To determine contact resistivity, four-point probe current–voltage (I–V) measurements were conducted using HP4145B semiconductor parameter analyzer.

The PL measurements were conducted by measuring the emission spectra of the samples with an Avantes AvaSpec HS-TEC CCD spectrometer coupled to an Avantes FC-IR600-1-ME-HTX fiber. The excitation source was LOTIS TII Nd:YAG laser set to 12.5 J of 532 nm emission. The incident laser beam was filtered with a Thorlabs FLH532-10 bandpass filter (full width of half maximum (FWHM) = 10 nm) before reaching the sample. The reflected emission was filtered with a Standa KS-17 long-pass filter before the detector. The measurement parameters in Avantes AvaSoft were scope minus dark mode, integration time 50 ms, 60 averages per measurement, and smoothing 0. For PL measurement, 1 nm thick Mg layer was deposited on p-InP and post heated.

Ab initio molecular dynamics simulations as implemented in the Vienna Ab Initio Simulation Package (VASP) were performed.[57–60] The calculations were based on the density functional theory (DFT) and Perdew–Burke–Ernzerhof (PBE) functional[61] within the projected augmented-wave method was used.[62,63] The Nose–Hoover thermostat (*NVT* ensemble) was used with a simulation step of 2 fs. The plane wave cutoff was 350 eV for most of the systems (300 and 400 eV for Ni and Mg, respectively). A single k point (Γ point) was used. About 100 atoms supercells were used. One interstitial atom was inserted into the supercells. For each case, several runs were carried out for 100–150 ps. Diffusional events were sparse in these systems. Therefore, numerical values for diffusivity were not given and the relative diffusivities were estimated by determining the number of ion hops between different crystal lattice sites. Diffusion was simulated at temperatures close to the melting points (but below them) due to the slow diffusion in the considered systems.

Supporting Information

Supporting Information is available from the Wiley Online Library or from the author.

Acknowledgements

This work was supported by the University of Turku Graduate School (UTUGS), the Academy of Finland (via the project #296469). The X-Ray photoelectron spectroscopy experiments were carried out using resources provided by MAterials Research Infrastructure (MARI). The computer resources of the Finnish IT Center for Science (CSC) are acknowledged.

Conflict of Interest

The authors declare no conflict of interest.

Data Availability Statement

The data that support the findings of this study are available from the corresponding author upon reasonable request.

Keywords

contact resistivity, p-InP, surface doping, wet chemistry

Received: May 22, 2023
Revised: July 13, 2023
Published online:

[1] X. F. Duan, Y. Huang, Y. Cui, J. F. Wang, C. M. Lieber, *Nature* **2001**, *409*, 66.
[2] J. Wang, M. S. Gudiksen, X. Duan, Y. Cui, C. M. Lieber, *Science* **2001**, *293*, 1455.
[3] T. E. Kazior, J. R. LaRoche, D. Lubyshev, J. M. Fastenau, W. K. Liu, M. Urteaga, W. Ha, J. Bergman, M. J. Choe, M. T. Bulsara, E. A. Fitzgerald, D. Smith, D. Clark, R. Thompson, C. Drazek, N. Daval, L. Benaissa, E. Augendre, in *IEEE MTT-S Int. Microw. Symp. Dig.* IEEE, Piscataway, NJ **2009**, 1113.
[4] J. Wallentin, N. Anttu, D. Asoli, M. Huffman, I. Åberg, M. H. Magnusson, G. Siefer, P. Fuss-Kailuweit, F. Dimroth, B. Witzigmann, H. Q. Xu, L. Samuelson, K. Deppert, M. T. Borgström, *Science* **2013**, *339*, 1057.
[5] C. Adelmann, D. Cuypers, M. Tallarida, L. N. J. Rodriguez, A. De Clercq, D. Friedrich, T. Conard, A. Delabie, J. W. Seo, J. P. Locquet, S. De Gendt, D. Schmeisser, S. Van Elshocht, M. Caymax, *Chem. Mater.* **2013**, *25*, 1078.
[6] Q. Gao, D. Saxena, F. Wang, L. Fu, S. Mokkapati, Y. Guo, L. Li, J. Wong-Leung, P. Caroff, H. H. Tan, C. Jagadish, *Nano Lett.* **2014**, *14*, 5206.
[7] X. Mei, W. Yoshida, M. Lange, J. Lee, J. Zhou, P. H. Liu, K. Leong, A. Zamora, J. Padilla, S. Sarkozy, R. Lai, W. R. Deal, *IEEE Electron Dev. Lett.* **2015**, *36*, 327.
[8] H. P. Wang, C. M. Sutter-Fella, P. Lobaccaro, M. Hettick, M. Zheng, D. H. Lien, D. W. Miller, C. W. Warren, E. T. Roe, M. C. Lonergan, H. L. Guthrey, N. M. Haegel, J. W. Ager, C. Carraro, R. Maboudian, Jr-H. He, A. Javey, *Chem. Mater.* **2016**, *28*, 4602.

[9] J. L. Zhang, P. Ding, B. Mei, S. H. Meng, C. Zhang, L. H. Ma, Z. Jin, Y. Sun, H. M. Zhang, Y. H. Zhong, *Appl. Phys. Lett.* **2022**, *120*, 103501.
[10] D. H. Shin, R. Lampande, S. J. Kim, Y. H. Jung, J. H. Kwon, *Adv. Electr. Mat.* **2022**, *8*, 2200256.
[11] L. Iemmo, A. Di Bartolomeo, F. Giubileo, G. Luongo, M. Passacantando, G. Niu, F. Hatami, O. Skibitzki, T. Schroeder, *Nanotechnology* **2017**, *28*, 495705.
[12] G. Niu, G. Capellini, F. Hatami, A. Di Bartolomeo, T. Niermann, E. H. Hussein, M. A. Schubert, H. M. Krause, P. Zaumseil, O. Skibitzki, G. Lupina, *ACS Appl Mater Interfaces* **2016**, *8*, 26948.
[13] J. C. Ho, R. Yerushalmi, Z. A. Jacobson, Z. Fan, R. L. Alley, A. Javey, *Nat. Mater.* **2008**, *7*, 62.
[14] D. Mocatta, G. Cohen, J. Schattner, O. Millo, E. Rabani, U. Banin, *Science* **2011**, *332*, 77.
[15] T. Haggren, G. Otnes, R. Mourão, V. Dagyte, O. Hultin, F. Lindelöw, M. Borgström, L. Samuelson, *J. Cryst. Growth* **2016**, *451*, 18.
[16] C. Cordoba, X. Zeng, D. Wolf, A. Lubk, E. Barrigón, M. T. Borgström, K. L. Kavanagh, *Nano Lett.* **2019**, *19*, 3490.
[17] C. S. Pang, T. Y. T. Hung, A. Khosravi, R. Addou, Q. Wang, M. J. Kim, R. M. Wallace, Z. Chen, *Adv. Electr. Mat.* **2020**, *6*, 190130.
[18] Y. Tan, W. Zhang, X. Xiao, J. Sun, J. Ma, T. Zhang, G. Mei, Z. Wang, F. Zhao, D. Wu, W. C. Choy, *Appl. Phys. Lett.* **2021**, *119*, 221105.
[19] Y. Zhu, V. Raj, Z. Li, H. H. Tan, C. Jagadish, L. Fu, *Adv. Mat.* **2021**, *33*, 2105729.
[20] E. Ber, R. W. Grady, E. Pop, E. Yalon, *Adv. Electron. Mater.* **2023**, 2201342.
[21] H. Nickel, E. Kuphal, *Phys. Status Solidi A* **1981**, *65*, 583.
[22] E. Kuphal, *Sol. State Electron.* **1981**, *24*, 69.
[23] S. N. G. Chu, R. A. Logan, M. Geva, N. T. Ha, *J. Appl. Phys.* **1995**, *78*, 3001.
[24] A. G. Baca, F. Ren, J. C. Zolper, R. D. Briggs, S. J. Pearton, *Thin Solid Films* **1997**, *308*, 599.
[25] P. A. Postigo, M. L. Dotor, P. Huertas, F. Garcıia, D. Golmayo, F. Briones, *J. Appl. Phys.* **1999**, *85*, 6567.
[26] B. Tuck, *J. Cryst. Growth* **2000**, *208*, 123.
[27] S. Hwang, J. Shim, Y. Eo, *J. Korean Phys. Soc.* **2005**, *46*, 751.
[28] A. M. Crook, E. Lind, Z. Griffith, M. J. Rodwell, J. D. Zimmerman, A. C. Gossard, S. R. Bank, *Appl. Phys. Lett.* **2007**, *91*, 192114.
[29] M. T. Björk, H. Schmid, J. Knoch, H. Riel, W. Riess, *Nat. Nanotechn.* **2009**, *4*, 103.
[30] A. P. Wijnheijmer, J. K. Garleff, K. Teichmann, M. Wenderoth, S. Loth, R. G. Ulbrich, P. A. Maksym, M. Roy, P. M. Koenraad, *Phys. Rev. Lett.* **2009**, *102*, 166101.
[31] W. Wilmsen, in *Physics and Chemistry of III-V Compound Semiconductor Interfaces*, Springer, New York **1985**.
[32] S. Oktyabrsky, P. D. Ye, in *Fundamentals of III-V Semiconductor MOSFETs*, Springer, New York **2010**.
[33] P. Laukkanen, M. P. J. Punkkinen, M. Kuzmin, K. Kokko, J. Lång, R. M. Wallace, *Appl. Phys. Rev.* **2021**, *8*, 011309.
[34] T. Zhao, Q. Zhao, J. Lee, S. Yang, H. Wang, M. Y. Chuang, Y. He, S. M. Thompson, G. Liu, N. Oh, C. B. Murray, C. R. Kagan, *Chem. Mater.* **2022**, *34*, 8306.
[35] R. F. Ubbink, G. Almeida, H. Iziyi, I. du Fossé, R. Verkleij, S. Ganapathy, E. R. H. van Eck, A. J. Houtepen, *Chem. Mater.* **2022**, *43*, 10093.
[36] H. J. Joyce, J. Wong-Leung, C. K. Yong, C. J. Docherty, S. Paiman, Q. Gao, H. H. Tan, C. Jagadish, J. Lloyd-Hughes, L. M. Herz, M. B. Johnston, *Nano Lett.* **2012**, *12*, 5325.
[37] M. Ebrahimzadeh, S. Vuori, M. Miettinen, J. P. Lehtiö, S. Granroth, M. P. J. Punkkinen, Z. J. Rad, R. Punkkinen, M. Kuzmin, P. Laukkanen, M. Lastusaari, K. Kokko, *J. Phys. D: Appl. Phys.* **2023**, *56*, 044001.
[38] A. Yamaguchi, H. Asamizu, T. Okada, Y. Iguchi, T. Saitoh, Y. Koide, M. Murakami, *J. Appl. Phys.* **1999**, *85*, 7792.
[39] D. G. Ivey, P. Jian, L. Wan, R. Bruce, S. Eicher, C. Blaauw, *J. Electron. Mater.* **1991**, *20*, 237.
[40] M. H. Park, L. C. Wang, J. Y. Cheng, F. Deng, S. S. Lau, C. J. Palmström, *Appl. Phys. Lett.* **1996**, *68*, 952.
[41] H. Asamizu, A. Yamaguchi, Y. Iguchi, T. Saitoh, Y. Koide, M. Murakami, *Appl. Surf. Sci.* **2000**, *159*, 174.
[42] S. E. Mohney, Y. A. Chang, *J. Appl. Phys.* **1993**, *74*, 4403.
[43] N. Szydlo, J. Olivier, *J. Appl. Phys.* **1979**, *50*, 1445.
[44] T. C. Hasenberg, E. Garmire, *J. Appl. Phys.* **1987**, *61*, 808.
[45] D. G. Ivey, P. Jian, R. Bruce, *J. Electron. Mater.* **1992**, *21*, 831.
[46] R. Caron-Popowich, J. Washburn, T. Sands, A. Kaplan, *J. Appl. Phys.* **1988**, *64*, 4909.
[47] T. Sands, C. C. Chang, A. S. Kaplan, V. G. Keramidas, K. M. Krishnan, J. Washburn, *Appl. Phys. Lett.* **1987**, *50*, 1346.
[48] A. Yamaguchi, H. Asamizu, T. Okada, Y. Iguchi, T. Saitoh, Y. Koide, M. Murakami, *J. Vac. Sci. Technol. B* **2000**, *18*, 1957.
[49] S. Lu, M. Deki, J. Wang, K. Ohnishi, Y. Ando, T. Kumabe, H. Watanabe, S. Nitta, Y. Honda, H. Amano, *Appl. Phys. Lett.* **2021**, *119*, 242104.
[50] W. G. Schmidt, P. H. Hahn, F. Bechstedt, N. Esser, P. Vogt, A. Wange, W. Richter, *Phys. Rev. Lett.* **2003**, *90*, 126101.
[51] F. Boyer, P. Gergaud, K. Dabertrand, D. Mariolle, C. Jany, F. Nemouchi, M. Grégoire, Q. Rafhay, P. Rodriguez, *J. Vac. Sci. Technol. B* **2020**, *38*, 012209.
[52] E. A. Irene, *Mater. Sci. Forum* **1995**, *185*, 37.
[53] Z. Feng, X. Qin, X. Chen, Z. Li, R. Huang, Y. Shen, D. Ding, Y. Wang, M. Jing, Y. Cui, A. Dingsun, H. Liu, H. Dong, R. M. Wallace, *Appl. Phys. Lett.* **2022**, *120,* 032103.
[54] A. P. Seitsonen, R. Virkkunen, M. J. Puska, R. M. Nieminen, *Phys. Rev. B.* **1994**, *49*, 5253.
[55] J. Chen, W. D. Brewer, *Adv. Electron. Mater.* **2015**, *1*, 1500113.
[56] C. M. Smyth, L. A. Walsh, P. Bolshakov, M. Catalano, M. Schmidt, B. Sheehan, R. Addou, L. Wang, J. Kim, M. J. Kim, C. D. Young, C. L. Hinkle, R. M. Wallace, *2D Mater.* **2019**, *6*, 045020.
[57] G. Kresse, J. Hafner, *Phys. Rev. B* **1993**, *47*, 558.
[58] G. Kresse, J. Hafner, *Phys. Rev. B* **1994**, *49*, 14251.
[59] G. Kresse, J. Furthmüller, *Comput. Mat. Sci.* **1996**, *6*, 15.
[60] G. Kresse, J. Furthmüller, *Phys. Rev. B* **1996**, *54*, 11169.
[61] J. P. Perdew, K. Burke, M. Ernzerhof, *Phys. Rev. Lett.* **1996**, *77*, 3865.
[62] P. E. Blöchl, *Phys. Rev. B* **1994**, *50*, 17953.
[63] G. Kresse, D. Joubert, *Phys. Rev. B* **1999**, *59*, 1758.
[64] L. P. Erickson, A. Waseem, G. Y. Robinson, *Thin Sol. Films* **1979**, *64*, 421.
[65] H. Temkin, R. J. McCoy, V. G. Keramidas, W. A. Bonner, *Appl. Phys. Lett.* **1980**, *36*, 444.
[66] A. J. Valois, G. Y. Robinson, *Solid State Electron.* **1982**, *25*, 973.
[67] J. B. Boos, W. Kruppa, *Solid State Electron.* **1988**, *31*, 127.
[68] T. Clausen, A. S. Pedersen, O. Leistiko, *Microelectron. Eng.* **1991**, *15*, 157.
[69] M. H. Park, L. C. Wang, D. M. Hwang, *J. Electron. Mater.* **1996**, *25*, 721.
[70] M. H. Park, L. C. Wang, J. Y. Cheng, C. J. Palmstrom, *Appl. Phys. Lett.* **1997**, *70*, 99.
[71] H. Asamizu, A. Yamaguchi, Y. Iguchi, T. Saitoh, M. Murakami, *Mater. Trans.* **2002**, *43*, 1352.
[72] S. Hwang, J. Shim, Y. Eo, in *Int. Conf. on Indium Phosphide and Related Materials*, **2005**, p. 260.
[73] M. D. Kim, J. M. Baek, T. G. Kim, S. G. Kim, K. S. Chung, *Thin Sol. Films* **2006**, *514*, 250.
[74] L. Han, C. Du, Z. Ma, Y. Jiang, K. Xiong, W. Wang, H. Chen, Z. Deng, H. Jia, *Chin. Phys. Lett.* **2021**, *38*, 068102.